


SCIENTIFIC REPORTS



OPEN

Direct visualization of charge transport in suspended (or free-standing) DNA strands by low-energy electron microscopy

Tatiana Latychevskaia¹ , Conrad Escher¹, William Andregg², Michael Andregg² & Hans-Werner Fink¹

Low-energy electrons offer a unique possibility for long exposure imaging of individual biomolecules without significant radiation damage. In addition, low-energy electrons exhibit high sensitivity to local potentials and thus can be employed for imaging charges as small as a fraction of one elementary charge. The combination of these properties makes low-energy electrons an exciting tool for imaging charge transport in individual biomolecules. Here we demonstrate the imaging of individual deoxyribonucleic acid (DNA) molecules at the resolution of about 1 nm with simultaneous imaging of the charging of the DNA molecules that is of the order of less than one elementary charge per nanometer. The cross-correlation analysis performed on different sections of the DNA network reveals that the charge redistribution between the two regions is correlated. Thus, low-energy electron microscopy is capable to provide simultaneous imaging of macromolecular structure and its charge distribution which can be beneficial for imaging and constructing nano-bio-sensors.

Charge transport through deoxyribonucleic acid (DNA) molecules has been a highly interesting (but also controversial) subject over the past few decades in view of the potential for building bio-nano-electronic devices^{1–3}. The reports about the electronic properties of DNA are highly controversial⁴. Time-resolved experiments reported ultrafast electron transfer in double stranded DNA (dsDNA) with time constants of 5 ps and 75 ps over 10–17 Å distance⁵. Kasumov *et al.* reported that dsDNA molecule exhibited ohmic behaviour between room temperature and 1 Kelvin with resistance per molecule less than 100 kilohm, and below 1 K proximity-induced superconductivity was observed⁶. Okahata *et al.* investigated electrical conductivity of in DNA-lipid complex film, where they measured electrical current in dsDNA- and almost no electrical current in single stranded DNA (ssDNA)-lipid complex films; these results imply that the conduction of ssDNA could be much less than the conduction of dsDNA⁷. Some DNA transport measurements indicated that DNA molecules could be conductive^{7–9}. Fink *et al.* measured that DNA molecules could act as a semiconductor exhibiting a resistivity of about 1 mΩ/cm⁸. Yoo *et al.* reported that poly(dA)-poly(dT) behaved as an n-type semiconductor, whereas poly(dG)-poly(dC) behaved as a p-type semiconductor⁹. Other experiments indicated that DNA could be insulating^{10–13}. An overview of possible mechanisms of charge transport through DNA is provided by Generaux and Barton¹.

Low-energy electrons with kinetic energies in the range 30–250 eV provide a unique type of radiation which causes no significant radiation damage to biological molecules, as was exemplified by continuous exposure of individual DNA molecules to low-energy electrons for 70 min, without noticeable change in their interference pattern (hologram)¹⁴. The number of electrons required to acquire a single 20 ms low-energy electron hologram at 1 nm resolution amounts to about 250 electrons per 1 Å², which translates into a radiation dose of 4.58×10^{11} Gray. This radiation dose exceeds the maximum tolerable dose for high-energy electrons and X-ray imaging by about a factor of 10⁴. The details of this calculations are provided in the Supplementary Information.

During the past two decades, low-energy electrons have successfully been applied for imaging of individual biological molecules, including: purple protein membrane¹⁵, DNA molecules^{16–18}, phthalocyaninato polysiloxane molecules¹⁹, the tobacco mosaic virus²⁰, a bacteriophage²¹, ferritin²² and individual proteins (bovine serum

¹Physics Department, University of Zurich, Winterthurerstrasse 190, 8057, Zurich, Switzerland. ²Halcyon Molecular, 505 Penobscot Drive, Redwood City, CA, 94063, USA. Correspondence and requests for materials should be addressed to T.L. (email: tatiana@physik.uzh.ch)

albumin, cytochrome C and hemoglobin)²³. Most of these results were obtained by imaging individual molecules stretched over holes in carbon films^{15–21}. However, such a sample arrangement creates an unwanted so-called biprism effect. Such biprism effect occurs when the electron wave passes by a positively charged wire, so that the electrons are deflected towards the wire²⁴. In light optics such effect can be created by adding a biprism phase distribution into the wavefront. In low-energy electron imaging even if the fiber is not charged, such biprism effect can occur due to the bending of the potential around the molecule resulting in a deflection of the electron trajectories similar to as if the molecule was charged²⁰. The biprism effect complicates the interpretation of the data record²⁵. Biprism effects can be reduced if the individual molecules are stretched over smaller holes in a carbon film. Simulations performed by Weierstall *et al.*²⁰ demonstrated that stretching an 18 nm fiber over a 100 nm instead of typical 1–2 micron holes, successfully suppresses the biprism effect. In this study we demonstrate low-energy electron imaging of individual DNA molecules that are stretched over holes in lacey carbon with hole sizes of just tens of nanometers.

Low-energy electrons exhibit high sensitivity to local potentials²⁶ allowing imaging individual charges as small as a fraction of an elementary charge^{27–29}. This is why low-energy electron imaging is a unique tool to probe charge effects in DNA molecules at high spatial resolution and at high sensitivity to the smallest amount of charge.

Sample Preparation

The sample consisted of individual single-stranded DNA (ssDNA) strands as well as bundles thereof stretched over holes in lacey carbon. The thymine bases in ssDNA were labelled with osmium atoms by staining ssDNA with a thymidine-selective osmium tetroxide 2–29 bipyridine (osbipy) contrast-enhancing label. The ssDNA strands were prepared by the “molecular threading” method - a surface independent tip-based method for stretching and depositing single and double-stranded DNA molecules³⁰. DNA was stretched into air at a liquid-air interface and subsequently deposited onto a dry substrate isolated from solution. A fluorescence microscopy image of such sample is shown in Fig. 1a.

Experimental Setup

The low-energy electron microscope employed in this study has been described in details in previous publications^{16,18,21–23,31} and is schematically shown in Fig. 1b. The source of the coherent electron beam was a sharp W(111) tip and the electrons were extracted by field emission³². The position of the tip was controlled by a 3-axis piezo-manipulator with nanometer precision. The wave transmitted through the sample propagated to the detector unit where the interference pattern is acquired, formed by superposition of the scattered with the non-scattered (reference) wave, constituting an in-line hologram^{33,34}. The detector unit consisted of a microchannel plate (MCP), a phosphor screen, and a digital camera. A typical inline hologram of ssDNA fibers acquired with this setup is shown in Fig. 1c, exhibiting ssDNA fibers perfectly stretched over the lacey carbon support. Examples of ssDNA holograms at different magnifications are provided in the Supplementary Information.

Results

Visualisation of charge redistribution. Figure 2 shows low-energy electron microscopy images of ssDNA. In each experiment, a sequence of holograms was recorded at a standard video rate (25 frames per second). An individual hologram (frame) is shown in Fig. 2a, where one can see ssDNA fibers stretched over holes in lacey carbon. Some ssDNA fibers exhibit brighter or darker regions, which is an indication of negative (darker regions) and positive (brighter regions) charge. The presence of charge affects the electron trajectories: negative charge deflects passing electrons away from the charge, while positive charge deflects passing electrons towards the charge thus creating a lens-like effect. A sequence of holograms of the same sample as shown in Fig. 2 is provided as a movie in Supplementary Movie 1. Part of the imaged sample contained only the carbon fibers without DNA fibers, marked by the yellow rectangles in Fig. 2a,b. From the Supplementary Movie 1, it is apparent that the intensity contrast is only varying along the DNA fibers, and no intensity contrast variations were observed along the carbon fibers in the regions marked by the yellow rectangle. We therefore can assume that the charge redistribution occurs only along the DNA fibers.

A somewhat blurry appearance of the experimental images (in Figs 2, 3, S2 and Supplementary Movies 1 and 2) can be explained as follows. When the electron source or the sample is laterally shifting, the image on the detector (hologram) is laterally shifting by the same amount of shift multiplied with the magnification of the system. For example, a sample shift by 1 Ångstrom leads to a hologram shift by 10 micron at a typical magnification of 10⁵. In addition, the fibers in the lacey samples are not mechanically rigid and can also exhibit deflections in the axial direction, which affect the magnification of the resulting images. Since the lateral and axial positions of the fibers are continuously varying (as it can be observed in Supplementary Movies 1 and 2), the resulting hologram of the fiber, averaged over the time period corresponding to the single frame acquisition time, appears blurry.

Quantitative estimation of charges. The high sensitivity of low-energy electrons to local potentials allows detecting smallest charges^{28,29}. The effect of electron trajectories deflections due to charges and their redistribution in biological samples is often discussed in biological single particle transmission electron microscopy imaging^{35,36}. In low-energy electron holography, due to this effect, the resulting in-line holograms of the molecules are affected by distortions, as shown in Fig. 2a,b in the cyan rectangle. The three ssDNA fibers in Fig. 2a,b in the cyan rectangle, indicated with two red and one blue arrows, are not physically bent towards each other, this is a distortion in the in-line hologram created by the electron trajectories that have been deflected due to the charges present on the molecules, as indicated by the bright (due to a positive charge) and dark (due to a negative charge) appearance of the ssDNA fibers. To illustrate this “bending” effect, a similar situation of three charged fibers separated by 100 nm was simulated. A linear charge distributed over the fiber was assumed, which creates a biprism phase-shifting distribution; the procedure of hologram simulations of fibers with linear charge is explained in

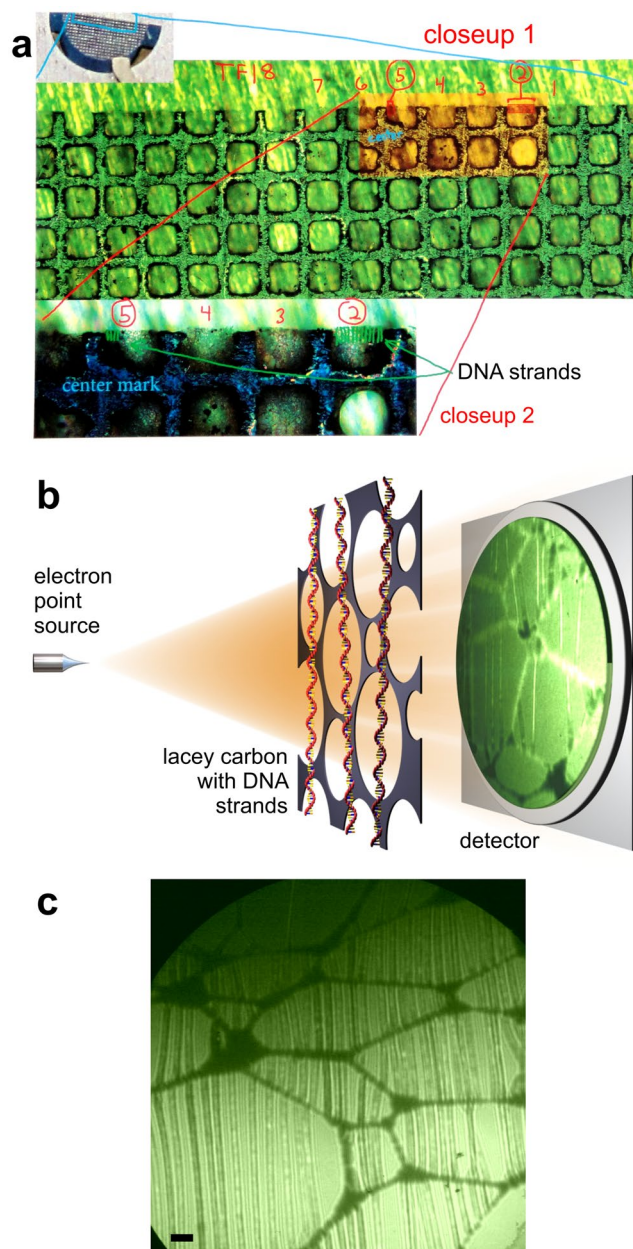


Figure 1. Imaging single-stranded DNA molecules by low-energy electron microscopy. (a) The sample imaged by fluorescence optical microscopy at different magnifications, where two compartments (2 and 5) containing individual DNA strands are indicated. (b) Schematics of the low-energy electron microscope where the sample can be imaged at different magnification, the electron source-to-sample distance can be varied from tens of nanometers to a few microns. (c) An in-line hologram of ssDNA fibers in compartment 2 as labelled in (a), acquired with electrons of 188 eV kinetic energy, at the distance between the electron source and the sample of about 100 μm . The scalebar corresponds to 100 nm.

ref.²⁵. A simulated hologram when the linear charge of the fibers is $Q = 0.1 \text{ e/nm}$, $+|Q|$ for the left and the center fibers and $-|Q|$ for the right fiber, is shown in Fig. 2c. The intensity profile through the simulated holograms at $Q = 0.05 \text{ e/nm}$ and $Q = 0.1 \text{ e/nm}$ are shown in Fig. 2d, together with the indicated actual positions of the fibers. It is apparent that the maxima and minima of the intensity in the holograms are significantly shifted, almost by 50% from the original fiber positions. It is also remarkable that such a huge shift is caused by such small charges, illustrating the high sensitivity of low-energy electrons to local charges.

Correlated charge redistribution. Figure 3 shows a study of the time evolution of the intensity fluctuations in the hologram of an ssDNA. A region selected for the analysis is indicated in Fig. 2a by the blue rectangle. The bottom left ssDNA fiber exhibits a biprism effect which is an indication of positive charging. The first 10 holograms (frames) of the region are shown in Fig. 3a. The normalized intensity as a function of time (frame

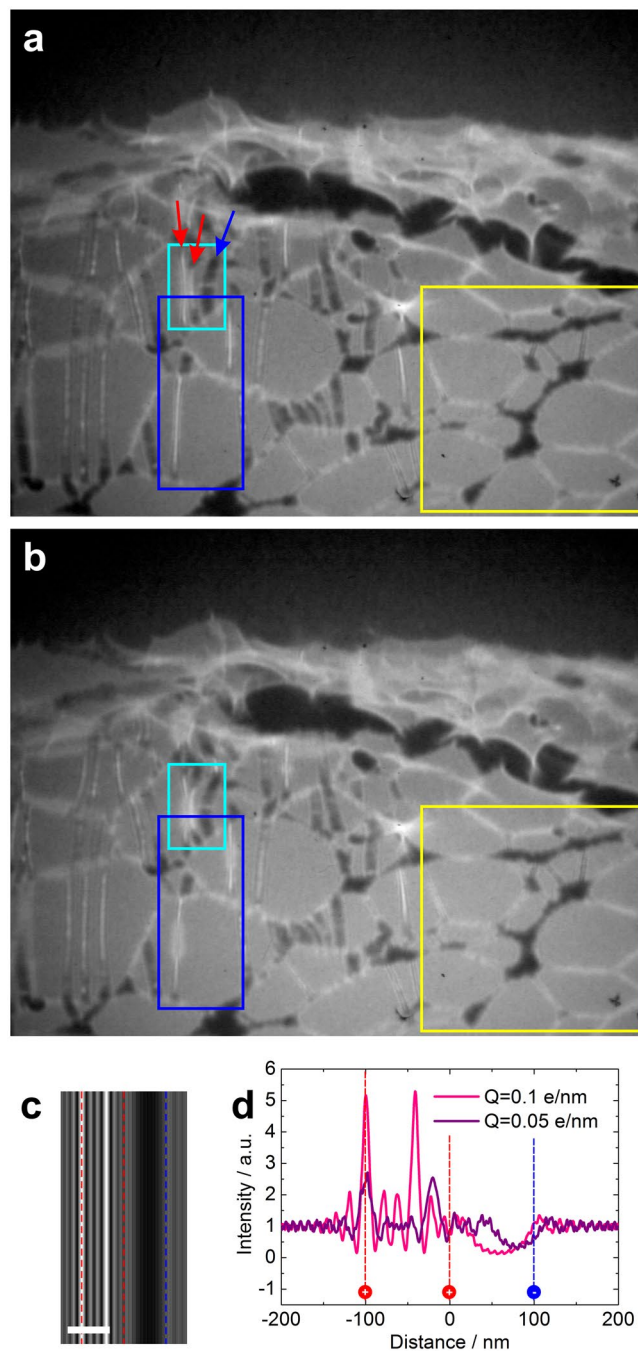


Figure 2. Low-energy electron microscopy of ssDNA. (a) Single hologram of ssDNA fibers suspended over holes in lacy carbon acquired with electrons of 215 eV energy and a 10 nA current. (b) Hologram of the same region as in (a), acquired 600 ms later. A complete movie, showing the time-dependent behaviour of this region under continuous exposure to electrons is provided as the Supplementary Movie 1. (c) Simulated hologram of three 2 nm thick fibers with the linear charge of the fibers is $|Q| = 0.1$ e/nm, $+|Q|$ for the left and the center fibers and $-|Q|$ for the right fiber. The distance between the fibers is 100 nm, the electron energy is 215 eV and the distance between the source and the sample is 10 μ m. The scalebar corresponds to 100 nm. (e) Intensity profiles through the simulated holograms of three charged fibers with $|Q| = 0.1$ e/nm and $|Q| = 0.05$ e/nm. The actual positions of the charged fibers are indicated by the dashed lines in (c) and (d).

number) at two selected sub-regions is shown in Fig. 3b. The intensity as a function of time (frame number) at two adjacent sub-regions is shown in Fig. 3c. The normalized intensity values at the selected sub-regions (indicated by the blue and the lilac arrows, respectively) were calculated as follows. The intensity is averaged over a 27×27 nm² area in the sub-region indicated by the solid arrow, giving I_i , $i = 1, 2$, respectively. An averaged intensity over a 27×27 nm² area in the reference sub-region indicated by the dotted arrow was also calculated, giving

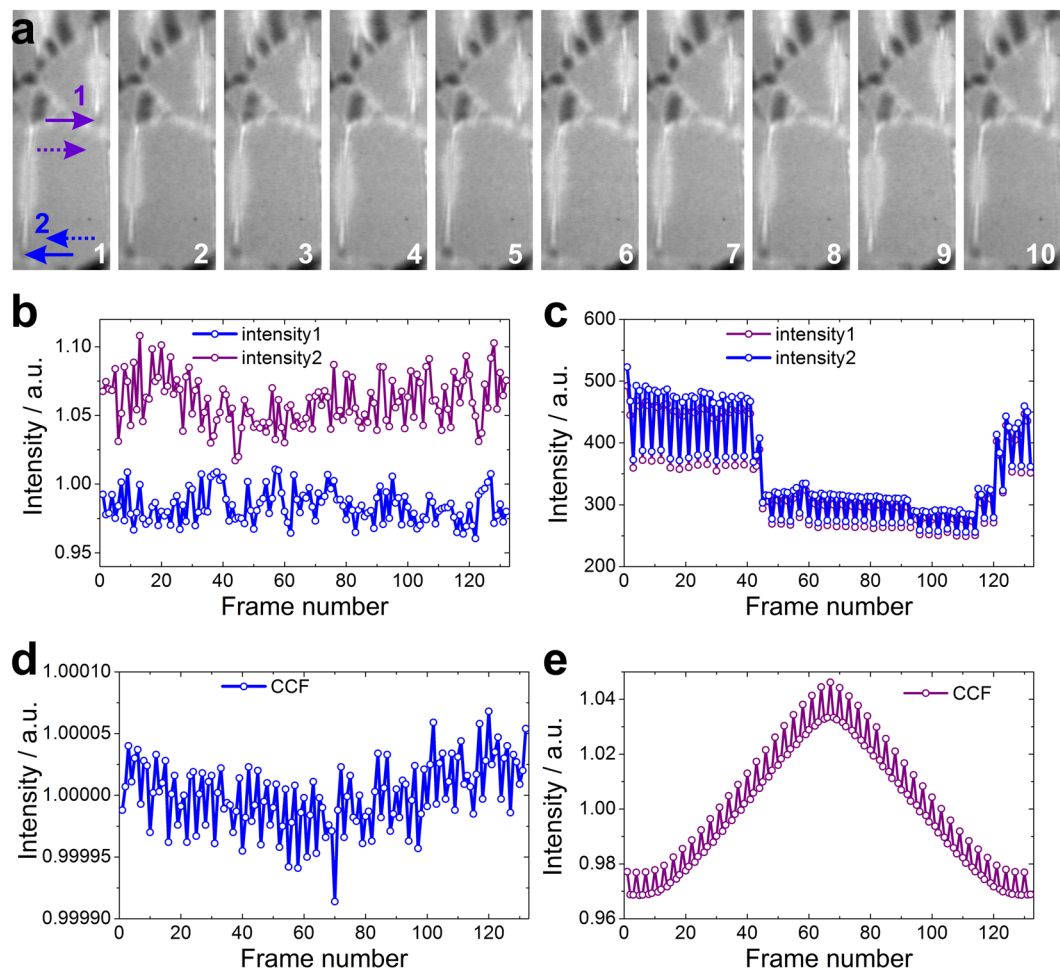


Figure 3. Time evolution of intensity fluctuations in a hologram of ssDNAs. (a) Selected area in the first ten frames of a sequence of 132 frames. The selected area is shown in Fig. 2a in the blue rectangle. The frame number is shown in the bottom right corner of each frame. Two selected sub-regions are indicated by the blue and the lilac arrows, respectively. Two corresponding reference regions are indicated by the blue and the lilac dotted arrows, respectively. (b) Normalized intensity as a function of time (frame number) at the sub-regions 1 and 2 as indicated by the colored arrows in (a). (c) Intensity as a function of time (frame number) at the reference sub-regions 1 and 2 as indicated by the dotted colored arrows in (a). (d) Cross-correlation function calculated between intensities at the sub-regions 1 and 2 (CCF). (e) Cross-correlation function of the intensities at the reference sub-regions (CCF_{ref}).

$I_i^{(\text{ref})}$, $i = 1, 2$, respectively. The normalized intensity was calculated as $I_i/I_i^{(\text{ref})}$, $i = 1, 2$, respectively. The cross-correlation function (CCF) between the normalized intensities at the sub-regions at 1 and 2 is shown in Fig. 3d. The CCF_{ref} of the intensities at the reference sub-regions is shown in Fig. 3e, exhibiting a periodical fluctuation and a broad maximum caused by the intensity drop between frames 45 and 115 (as shown in Fig. 3c). These CCF_{ref} features are not present in CCF of the normalized intensities shown in Fig. 3d, though the CCF of the normalized intensities still shows some oscillations. Another remarkable difference between the two CCFs is that the CCF of the normalized intensities exhibits a minimum at frame = 0, thus indicating that there is a time shift between the two intensity distributions, as if the two intensity distributions can be described by cosine functions that are shifted by π relatively to one another. The CCF distribution and the time shift implies that the charge redistribution between the two regions is not completely random but correlated.

DNA molecules structure reconstruction. Figure 4 shows in-line low-energy electron holograms of ssDNA fibers and their reconstructions. In the holograms, one can notice bright blobs along the fibers (in particular in Fig. 4b), which can be associated with a small amount of localized positive charges. These charges demonstrate small oscillation-like movements around their position over time, as can be viewed in the Supplementary Movie 2. The reconstructions were obtained by numerical procedure as described elsewhere³⁷. The width of the fibers were evaluated from the reconstructions and amount for fiber D to: 4.57 ± 0.51 nm, and fiber E to: 6.60 ± 0.51 nm. This implies that fibers D and E are rather a bundle than individual ssDNA molecules. The individual thymine bases that are labelled by Osmium cannot be resolved in the obtained reconstructions.

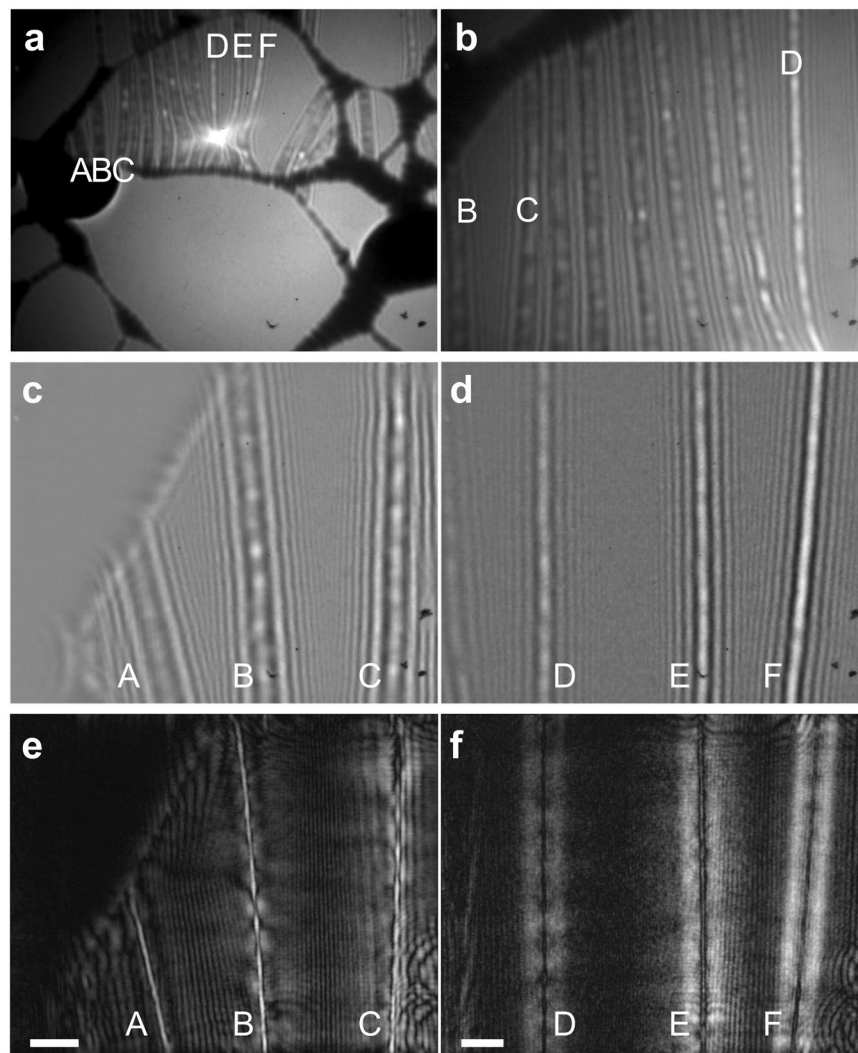


Figure 4. Low-energy electron holograms of ssDNA fibers and their reconstructions. **(a)** Overview image of a section of ssDNA fibers suspended over holes in lacey carbon, acquired with electrons of 154 eV energy and a 5 nA current. **(b)** Magnified image of the same region, acquired at a shorter electron source- to-sample distance, with electrons of 110 eV energy and a 400 pA current. Time-dependent behaviour of this region under continuous exposure to electrons is provided as the Supplementary Movie 2. **(c)** and **(d)** Magnified regions with ssDNA fibers A, B, C, D, E, and F acquired with electrons of 110 eV energy and a 350 pA current, at a distance between the source and the sample of 4.9 μm and 5.6 μm , respectively. **(e)** and **(f)** sample distributions obtained by reconstruction of the holograms shown in **(c)** and **(d)**. The scalebars in **(e)** and **(f)** correspond to 50 nm.

Figure 4a shows an in-line low-energy electron hologram of ssDNA fibers with three fibers seemingly merging together into a bright spot. This is another manifestation of the “bending effect” discussed above. Due to the presence of a strong positive charge on the middle fiber D, the electron trajectories are bent towards the positive charge, thus creating on the detector an image of bent neighbouring fibers.

Discussion and Conclusions

In conclusion, our results demonstrate that low-energy electron microscopy allows imaging of structure of biological macromolecules at about 1 nm spatial resolution and simultaneous imaging of its charge distribution at the resolution of sub elementary charges. Although biological samples are known to undergo charging effects under electron imaging, only with low-energy electrons this charging can directly be visualized.

Our experiments demonstrated that a region of the sample which contains only carbon fibers does not exhibit such intensity fluctuations as the nearby region of the sample which contains DNA molecules. We therefore conclude that we observe charge redistribution within DNA. The subject of DNA conductivity is highly controversial and we do not have an explanation about the exact mechanism of charge redistribution in DNA. We can only speculate that in our experiments the situation could be similar to that in graphene: although graphene is highly conductive in theory, in practise graphene has defects (missing atoms, adatoms etc) which affect the conductivity

severely. Adatoms on graphene can produce a local charge transfer³⁸, where the local charge can exhibit fluctuations in time²⁸.

We show that a charged ssDNA fiber can lead to a shift by a few tens of nanometers of the fiber's image (hologram) from its original position. For the ssDNA network, the cross-correlation analysis reveals that the charge redistribution between the two regions in the network that are tens of nanometers apart is not completely random but correlated. This result can potentially be useful for employing ssDNA networks in molecular electronics. Overall, low-energy electron microscopy offers a unique visualization tool for studying the charge transport in DNA and other biomolecules which could be potentially applied for the construction of nano-bio-sensors.

References

1. Genereux, J. C. & Barton, J. K. Mechanisms for DNA charge transport. *Chem. Rev.* **110**, 1642–1662 (2010).
2. Metzger, R. M. Unimolecular electronics. *Chem. Rev.* **115**, 5056–5115 (2015).
3. Xiang, D., Wang, X. L., Jia, C. C., Lee, T. & Guo, X. F. Molecular-scale electronics: from concept to function. *Chem. Rev.* **116**, 4318–4440 (2016).
4. Endres, R. G., Cox, D. L. & Singh, R. R. P. Colloquium: The quest for high-conductance DNA. *Rev. Mod. Phys.* **76**, 195–214 (2004).
5. Wan, C. Z. *et al.* Femtosecond dynamics of DNA-mediated electron transfer. *Proc. Natl. Acad. Sci. USA* **96**, 6014–6019 (1999).
6. Kasumov, A. Y. *et al.* Proximity-induced superconductivity in DNA. *Science* **291**, 280–282 (2001).
7. Okahata, Y., Kobayashi, T., Nakayama, H. & Tanaka, K. DNA-aligned cast film and its anisotropic electron conductivity. *Supramol. Sci.* **5**, 317–320 (1998).
8. Fink, H.-W. & Schonberger, C. Electrical conduction through DNA molecules. *Nature* **398**, 407–410 (1999).
9. Yoo, K. H. *et al.* Electrical conduction through poly(dA)-poly(dT) and poly(dG)-poly(dC) DNA molecules. *Phys. Rev. Lett.* **87**, 198102 (2001).
10. Braun, E., Eichen, Y., Sivan, U. & Ben-Yoseph, G. DNA-templated assembly and electrode attachment of a conducting silver wire. *Nature* **391**, 775–778 (1998).
11. Porath, D., Bezryadin, A., de Vries, S. & Dekker, C. Direct measurement of electrical transport through DNA molecules. *Nature* **403**, 635–638 (2000).
12. de Pablo, P. J. *et al.* Absence of dc-conductivity in lambda-DNA. *Phys. Rev. Lett.* **85**, 4992–4995 (2000).
13. Storm, A. J., van Noort, J., de Vries, S. & Dekker, C. Insulating behavior for DNA molecules between nanoelectrodes at the 100 nm length scale. *Appl. Phys. Lett.* **79**, 3881–3883 (2001).
14. Germann, M., Latychevskaia, T., Escher, C. & Fink, H.-W. Nondestructive imaging of individual biomolecules. *Phys. Rev. Lett.* **104**, 095501 (2010).
15. Spence, J., Qian, W. & Zhang, X. Contrast and radiation-damage in point-projection electron imaging of purple membrane at 100-V. *Ultramicroscopy* **55**, 19–23 (1994).
16. Fink, H.-W., Schmid, H., Ermantraut, E. & Schulz, T. Electron holography of individual DNA molecules. *J. Opt. Soc. Am. A* **14**, 2168–2172 (1997).
17. Eisele, A., Voelkel, B., Grunze, M. & Golzhauser, A. Nanometer resolution holography with the low energy electron point source microscope. *Z. Phys. Chem.* **222**, 779–787 (2008).
18. Latychevskaia, T., Longchamp, J.-N., Escher, C. & Fink, H.-W. In *Present and Future Methods for Biomolecular Crystallography* 331–342 (Springer, 2013).
19. Golzhauser, A. *et al.* Holographic imaging of macromolecules. *J. Vac. Sci. Technol. A* **16**, 3025–3028 (1998).
20. Weierstall, U., Spence, J. C. H., Stevens, M. & Downing, K. H. Point-projection electron imaging of tobacco mosaic virus at 40 eV electron energy. *Micron* **30**, 335–338 (1999).
21. Stevens, G. B. *et al.* Individual filamentous phage imaged by electron holography. *Eur. Biophys. J.* **40**, 1197–1201 (2011).
22. Longchamp, J.-N., Latychevskaia, T., Escher, C. & Fink, H.-W. Non-destructive imaging of an individual protein. *Appl. Phys. Lett.* **101**, 093701 (2012).
23. Longchamp, J.-N. *et al.* Imaging proteins at the single-molecule level. *PNAS* **114**, 1474–1479 (2017).
24. Mollenstedt, G. & Duker, H. Beobachtungen und Messungen an Biprisma-Interferenzen mit Elektronenwellen. *Zeitschrift Fur Physik* **145**, 377–397 (1956).
25. Latychevskaia, T., Longchamp, J.-N., Escher, C. & Fink, H.-W. On artefact-free reconstruction of low-energy (30–250 eV) electron holograms. *Ultramicroscopy* **145**, 22–27 (2014).
26. Muller, M., Kravtsov, V., Paarmann, A., Raschke, M. B. & Ernstorfer, R. Nanofocused plasmon-driven sub-10 fs electron point source. *ACS Photonics* **3**, 611–619 (2016).
27. Muller, M., Paarmann, A. & Ernstorfer, R. Femtosecond electrons probing currents and atomic structure in nanomaterials. *Nat. Commun.* **5**, 5292 (2014).
28. Latychevskaia, T., Wicki, F., Longchamp, J.-N., Escher, C. & Fink, H.-W. Direct observation of individual charges and their dynamics on graphene by low-energy electron holography. *Nano Lett.* **16**, 5469–5474 (2016).
29. Latychevskaia, T., Wicki, F., Escher, C. & Fink, H.-W. Imaging the potential distribution of individual charged impurities on graphene by low-energy electron holography. *Ultramicroscopy* **182**, 276–282 (2017).
30. Payne, A. C. *et al.* Molecular threading: Mechanical extraction, stretching and placement of DNA molecules from a liquid-air interface. *PLoS One* **8**, e69058 (2013).
31. Fink, H.-W., Stocker, W. & Schmid, H. Holography with low-energy electrons. *Phys. Rev. Lett.* **65**, 1204–1206 (1990).
32. Fink, H.-W. Point-source for ions and electrons. *Physica Scripta* **38**, 260–263 (1988).
33. Gabor, D. A new microscopic principle. *Nature* **161**, 777–778 (1948).
34. Gabor, D. Microscopy by reconstructed wave-fronts. *Proc. R. Soc. A* **197**, 454–487 (1949).
35. Curtis, G. H. & Ferrier, R. P. Electric charging of electron-microscope specimens. *J. Phys. D - Appl. Phys.* **2**, 1035–1040 (1969).
36. Russo, C. J. & Henderson, R. Charge accumulation in electron cryomicroscopy. *Ultramicroscopy* **187**, 43–49 (2018).
37. Latychevskaia, T. & Fink, H.-W. Practical algorithms for simulation and reconstruction of digital in-line holograms. *Appl. Optics* **54**, 2424–2434 (2015).
38. Liu, X. J. *et al.* Metals on graphene: interactions, growth morphology, and thermal stability. *Crystals* **3**, 79–111 (2013).

Author Contributions

W.A. and M.A. prepared the ssDNA samples, H.W.F. and C.E. performed the experiments, T.L. analyzed the data and wrote the initial draft of the paper, all authors participated in discussing and finalizing the manuscript.

Additional Information

Supplementary information accompanies this paper at <https://doi.org/10.1038/s41598-019-45351-4>.

Competing Interests: The authors declare no competing interests.

Publisher's note: Springer Nature remains neutral with regard to jurisdictional claims in published maps and institutional affiliations.



Open Access This article is licensed under a Creative Commons Attribution 4.0 International License, which permits use, sharing, adaptation, distribution and reproduction in any medium or format, as long as you give appropriate credit to the original author(s) and the source, provide a link to the Creative Commons license, and indicate if changes were made. The images or other third party material in this article are included in the article's Creative Commons license, unless indicated otherwise in a credit line to the material. If material is not included in the article's Creative Commons license and your intended use is not permitted by statutory regulation or exceeds the permitted use, you will need to obtain permission directly from the copyright holder. To view a copy of this license, visit <http://creativecommons.org/licenses/by/4.0/>.

© The Author(s) 2019